Development of Human-Body Model THUMS Version 6 containing Muscle Controllers and Application to Injury Analysis in Frontal Collision after Brake Deceleration

Daichi Kato, Yuko Nakahira, Noritoshi Atsumi, Masami Iwamoto

Abstract We developed a family of human-body finite-element models named THUMS Version 6 by incorporating one-dimensional multiple-muscle models into a family of detailed models of THUMS Version 4 based on medical image data for the prediction of occupant posture changes before a vehicle crash and injury risks during the crash. THUMS Version 6 has three body sizes: AM50, AF05, and AM95. A muscle-activation controller was applied in THUMS Version 6 for representing the muscle conditions of sleeping, relaxed, and braced drivers. The direct impact and compression response characteristics of the models were validated by comparison with cadaver test data, and the kinematic response characteristics considering muscle activation were validated by comparison with sled test data using volunteers. We performed simulations of a frontal collision with a velocity of 55 km/h after a deceleration of 0.8 G by autonomous emergency brakes for 300 ms, and the results showed that injury outcomes differed among the three muscle conditions and three body sizes. In addition, the effect of seatbelt pre-pretension was discussed in comparison with the braced condition. The simulation results obtained using THUMS Version 6 suggest the importance of considering muscle activity in injury prediction through simulated vehicle collisions.

Keywords frontal collision, human-body finite-element model, injury risk, muscle activation, seatbelt pre-pretension

I. INTRODUCTION

Current and future commercial vehicles worldwide are being equipped with advanced vehicle safety technologies such as autonomous emergency brakes (AEBs). AEBs help reduce risks of injury due to collisions. On the other hand, deceleration due to AEBs affects the occupant posture before collisions and, consequently, the occupant kinematics during collisions. Furthermore, a previous study [1] showed that the conditions of muscle activation of the occupant could affect the kinematics and mechanical responses during the deceleration due to AEBs. Therefore, for evaluating occupant injury risks in frontal collision after AEB operation, it is critical to consider the effect of muscle activity.

Volunteer tests on frontal impacts to measure the kinematics of occupants with different conditions of muscle activation, such as relaxed or braced conditions, were conducted in [1-2]. Such volunteer tests are useful for investigating occupant kinematics with muscle activation in a collision. However, they are not suitable for parametric studies on the effects of muscle activity on occupant kinematics. On the other hand, simulations using a human-body finite-element (FE) model are useful for such parametric studies.

Predictions of occupant injury risks in frontal collisions have been performed using several FE models, which include crash-test-dummy FE models such as the Test device for Human Occupant Restraint - New Technology (THOR-NT) dummy FE model [3] and human-body FE models such as Total HUman Model for Safety (THUMS) Version 4 [4] and the Global Human Body Models Consortium (GHBMC) detailed model [5]. THUMS Version 4 was used to examine chest-injury risks in frontal collisions in [6]. The GHBMC detailed model was used to evaluate the effect of simulated pre-crash braking in [7]. These human-body models are detailed FE models developed based on medical imaging data such as computed tomography (CT) scan data, and the number of elements in the whole body is approximately two million in these models. However, since these models do not include activable muscle models, they are not used to investigate the effects of muscle activity during deceleration before a crash on injury risks.

D. Kato is an Associate Researcher (Phone: +81-561-71-7605; E-mail: d-kato@mosk.tytlabs.co.jp), Y. Nakahira is a Senior Researcher, N. Atsumi is an Associate Researcher, and M. Iwamoto is a Senior Researcher at the Human Science Research-Domain, Toyota Central R&D Labs., Inc., Japan.

On the other hand, human-body models with active muscles have been developed by several studies. A multi-body human model including the muscles of the neck, arms, and legs was developed in [8]. In this model, each human-body part was modelled as a rigid body, each joint was modelled as a mechanical joint, and each muscle was modelled using Hill-type muscle elements. The multi-body human model is advantageous in terms of computational costs, but it cannot be used for injury analysis in bones, ligaments, and internal organs. An active human-body FE model with some muscles in the neck, trunk, and upper extremities was developed in [9] by incorporating the muscles modelled using Hill-type muscle elements into a human-body model, THUMS Version 3 [10]. However, the active human-body model is not suitable for the accurate prediction of internal-organ injuries and ligament ruptures, because it does not include internal organs and some of its joints are replaced by rigid-body joints. Therefore, THUMS Version 5, which includes the bones, skin, internal organs, brain, ligaments, and muscles, was developed in [11]. The muscles of THUMS Version 5 were modelled by one-dimensional (1D) bar elements with Hill-type muscle material characteristics, and each muscle has the capability of generating muscular forces. A total of 262 skeletal muscles — 23 neck muscles, 47 arm muscles, 9 trunk muscles, and 52 leg muscles on one-side — were modelled. In addition, the authors constructed a control system for muscle activation in THUMS Version 5 to simulate the kinematics of occupants under different conditions of muscle activation [12]. THUMS Version 5 could be used to investigate the effects of muscle activity on the general kinematics and injury risks of occupants before and during a crash. However, the total number of elements of THUMS Version 5 is approximately 280,000, which is one-eighth of that of THUMS Version 4. A human-body model that expresses the structure of the human body in detail with many more elements and has activable multiple-muscle models is necessary for more detailed injury risk analyses of occupants under different conditions of muscle activation.

The purpose of the present study was to develop a human-body model, including both a detailed human-body structure and activable muscles, for predicting occupant injury risks in frontal collisions with deceleration before the crash and to apply the developed model to injury analysis in such conditions.

II. METHODS

This study used LS-DYNA^{TM} R9.2 (Livermore Software Technology Corporation, USA) for developing the models and conducting simulations using the models. LS-DYNA is a general-purpose multi-physics simulation software package including a nonlinear explicit FE solver.

Human-Body FE Model THUMS Version 6

We developed a human-body model called THUMS Version 6, as shown in Figure 1. The model has three different body sizes corresponding to a 50th-percentile adult male (AM50, with a height of 179 cm and weight of 79 kg), a 5th-percentile adult female (AF05, with a height of 153 cm and weight of 49 kg), and a 95th-percentile adult male (AM95, with a height of 188 cm and weight of 106 kg).

THUMS Version 4 [4] included detailed body-part models based on a high-precision CT-scan dataset and was used to predict bone fractures, ligament ruptures, and damage to the brain and internal organs. On the other hand, THUMS Version 5 [11] was developed by updating THUMS Version 3 [10] with major modifications including the implementation of whole-body skeletal muscles. THUMS Version 6 was developed by incorporating the muscle models of Version 5 into Version 4. The total numbers of elements in AM50, AF05, and AM95 of Version 6 are approximately 1.9, 2.5, and 2.0 million, respectively. The muscles are modelled by 1D bar elements with Hill-type muscle characteristics, and the models can generate muscular forces based on given activation levels of muscles. THUMS Version 6 has both a detailed human-body structure and activable muscles.

The geometric arrangements of muscle paths of THUMS Version 6 were validated using the muscle moment arm data taken from the literature, and the maximum voluntary joint torques were validated using volunteer test data taken from the literature. These validation methods and the data used for validations are the same as in the validations of muscle models of THUMS Version 5 [11].

The muscle parameters of AF05 were set differently from those of the male models. The physiological cross-sectional area (PCSA) of each muscle could significantly affect the muscular force. The PCSAs of AM50 were primarily determined based on [13]. However, the PCSAs of one-third of all muscles were determined based on the muscle cross-sectional areas measured from a male subject of the Visible Human Project Data

(National Institutes of Health, USA), because the PSCA data of small muscles in the hands, feet and neck are not included in [13]. Referring to the muscle models in a previous study [14], the muscular PCSAs of AF05 were set to be smaller than those of AM50. The PCSAs of AF05 were calculated by using ratios of the measured cross-sectional areas of a female subject to those of a male subject from the Visible Human Project Data. In addition, the PCSAs of AM95 were assumed to be the same as those of AM50. The PCSA data of major muscles are listed in Table I.

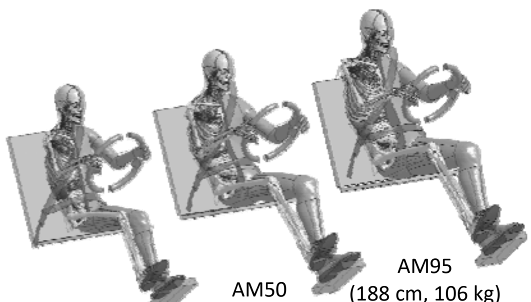

Fig. 1. Occupant models of THUMS Version 6.

TABLE I
PCSA DATA OF MAJOR MUSCLE MODELS

Body part	Muscle name	PCSA (mm^2)		Ratio (%)
		Male	Female	Female/Male
Neck	Sternocleidomastoid	492.00	313.60	63.74
	Longus Colli	82.80	49.20	59.42
	Splenius Capitis	494.40	312.00	63.11
	Semispinalis Capitis	552.00	327.20	59.28
Shoulder	Levator Scapulae	993.00	852.80	85.88
	Trapezius	2323.00	993.30	42.76
	Deltoid	2282.00	1985.20	86.99
	Pectoralis Major	1179.00	521.70	44.25
Upper Arm	Biceps Brachii Long Head	450.00	252.10	56.02
	Brachialis	881.00	274.70	31.18
Lower Arm	Flexor Carpi Ulnaris	557.00	461.50	82.85
	Extensor Digitorum	430.00	264.00	61.40
	Flexor Carpi Radialis	310.00	276.00	89.03
Abdomen	Rectus Abdominis	1050.00	548.70	52.26
	External Oblique	1027.56	328.80	32.00
Hip	Gluteus Medius	2000.00	1882.20	94.11
	Gluteus Maximus	2300.00	1841.10	80.05
Upper Leg	Sartorius	258.00	229.00	88.76
	Vastus Medialis	2625.00	1360.80	51.84
	Vastus Lateralis	4044.50	3409.70	84.30
Lower Leg	Tibialis Anterior	1268.00	382.90	30.20
	Flexor Digitorum Longus	613.00	573.60	93.57
	Extensor Digitorum Longus	628.00	414.80	66.05

Muscle-Activation Control of THUMS

When a driver is exposed to deceleration due to braking or impact, the driver is supposed to have several reactions to changes in velocity. If a driver does not anticipate the braking or impact, they may unconsciously perform some reflective action to reverse the posture changes due to the deceleration. If a driver anticipates the braking or impact, they may brace themselves by pushing the steering wheel and pressing the pedal or footrest. In this study, the former is called a relaxed driver, and the latter is called a braced driver.

The muscle conditions of relaxed and braced drivers are represented by a muscle-activation controller we developed in a previous study [12]. Figure 2 shows a diagram of the muscle-activation controller. The controller is applied in parallel with FE analysis using THUMS, and it decides the activation levels of muscles based on the displacement and force obtained from the FE analysis in each time step. The controller consists of two closed-loop feedback controls – one for posture control and the other for force control – and uses the proportional-integral-derivative (PID) control method. The posture control works to maintain the initial posture, and the force control works to reproduce the forces exerted by braced drivers to support their body. The muscle condition for the relaxed driver is represented using only the posture control, while that for the braced driver is represented using both the posture and force control.

According to [23], the reflex reaction of muscles is depressed in Non REM (Rapid Eye Movement) sleep relative to that in wakefulness and that is abolished in REM sleep. Therefore we assumed a sleeping driver as a driver without muscle activation, in which 0% of the activation levels were set to all muscles. This setting is also used for comparison with cadavers.

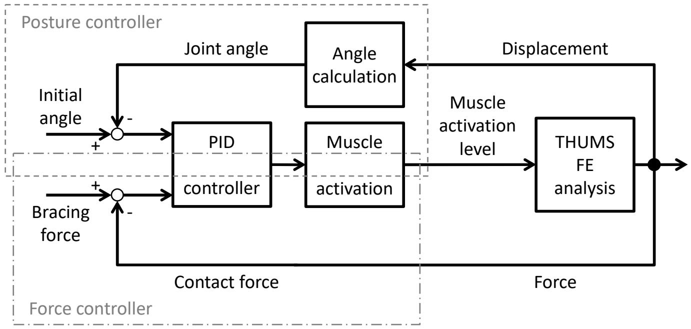

Fig. 2. Muscle-activation controller for THUMS.

TABLE II
CADAVERIC TEST DATA USED IN VALIDATION

Test condition	Reference
Thoracic frontal impact	[15]
Thoracic lateral impact	[16-17]
Thoracic-belt compression	[18]
Abdominal frontal impact	[19]
Abdominal-belt compression	[20]
Shoulder impact	[21]
Knee frontal impact	[22]

Validation of THUMS Version 6

Impact and Compression Responses

The impact and compression responses of the body parts of THUMS Version 6 were validated against seven series of cadaveric test data on direct impact or loading, as listed in Table II. These seven validation analyses using the three body models of THUMS Version 6 demonstrated that the simulation results for deflection and force showed almost similar tendencies to cadaveric test data. These results did not differ significantly from those of THUMS Version 4 [4], which does not include the muscles. Since we focus on the injury analyses during frontal collisions in this study, the details of validation analyses against the five conditions listed in Table II — thoracic frontal impact, thoracic-belt compression, abdominal frontal impact, abdominal-belt compression, and knee frontal impact — are presented in Appendix. In these analyses, the activation levels of all muscles were set to 0% for comparison with cadavers.

Kinematic Response Considering Active Portion

The muscle-activation controller was applied to AM50 of THUMS Version 6, and the kinematic response of THUMS and the influence of muscle activation on the kinematics were validated against a series of sled tests data using volunteers and cadavers.

The authors of [24] conducted a series of frontal sled tests involving five male volunteers with a body size approximately equal to that of AM50 and three male cadavers. The peak decelerations of the sled were 5 G and 2.5 G, which are equivalent to collisions at 9.7 km/h and 4.8 km/h, respectively. Each volunteer was exposed to two sled impulses under the two muscle conditions, i.e., relaxed and braced conditions. In the tests, all subjects sat on a rigid seat equipped with a three-point seatbelt, placing their feet on the footplates and their hands on the steering wheel. Occupant motions during decelerations were measured using a three-dimensional motion-capturing system. Simulation setups were reproduced using THUMS to be similar to the abovementioned experimental setups, as shown in Figure 3.

The muscle-activation controller requires the tuning of PID gains to be applied to the human-body models. In this study, we applied the PID gains tuned through our previous studies [12][25], which used THUMS Version 5 in low-speed frontal-impact conditions. The gains were determined by trial-and-error calculation to adjust occupant behaviour in the previous studies. First, the gains of posture control were determined by comparison with a relaxed volunteer, and the gains of force control were determined by comparison with a braced volunteer. These PID gains are listed in Table III. Since the time-delay function had not been implemented in the muscle-activation controller, the neural delay could not be represented.

We validated the kinematic response and the influence of muscle activation by comparing excursions of the head's centre of gravity (CG) with respect to the seat because we considered that head excursion is critical to understanding occupant kinematics in frontal crashes. Figure 4 shows head-CG excursions in the forward and downward directions during decelerations of 5 G. Simulation results were compared with volunteer test data taken from [24]. The relaxed and braced drivers represented using the muscle-activation controller were compared with the relaxed and braced volunteer, respectively. On the other hand, the data for the driver without muscle activation was compared with the cadaver data. Figure 4(a) shows that the head excursion of the cadaveric simulation was generally within the range of dispersion of cadaver data. Figure 4(b) shows that, in the relaxed simulation, the head CG displaced first forward and then downward, generally agreeing with volunteer data. Figure 4(c) shows that, in the braced simulation, the head CG tended to have a linear downward displacement, which was similar to the tendency in volunteer data. However, the displacement in the braced simulation was greater than that in volunteer data.

Furthermore, for the decelerations of 2.5 G, the simulation results of head excursions generally agreed with the test data.

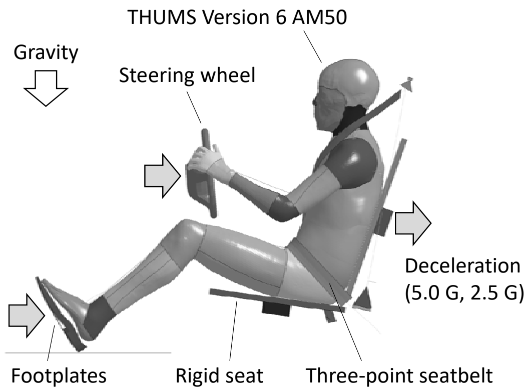

Fig. 3. Simulation setup to reproduce the frontal sled tests.

TABLE III
PID GAINS USED IN MUSCLE-ACTIVATION CONTROLLER [25]

Control	Body part	P gain	I gain	D gain
Posture	Neck and trunk	8 (rad^{-1})	0 ($rad^{-1} s^{-1}$)	Neck: 0.3 (s/rad) Trunk: 0 (s/rad)
	Lower extremity	1 (rad^{-1})	0 ($rad^{-1} s^{-1}$)	0 (s/rad)
	Upper extremity	2 (rad^{-1})	0 ($rad^{-1} s^{-1}$)	Elbow: 0.3 (s/rad) Others: 0 (s/rad)
Force	Hands and feet	0.002 (N^{-1})	0.1 ($N^{-1} s^{-1}$)	0 (s/N)

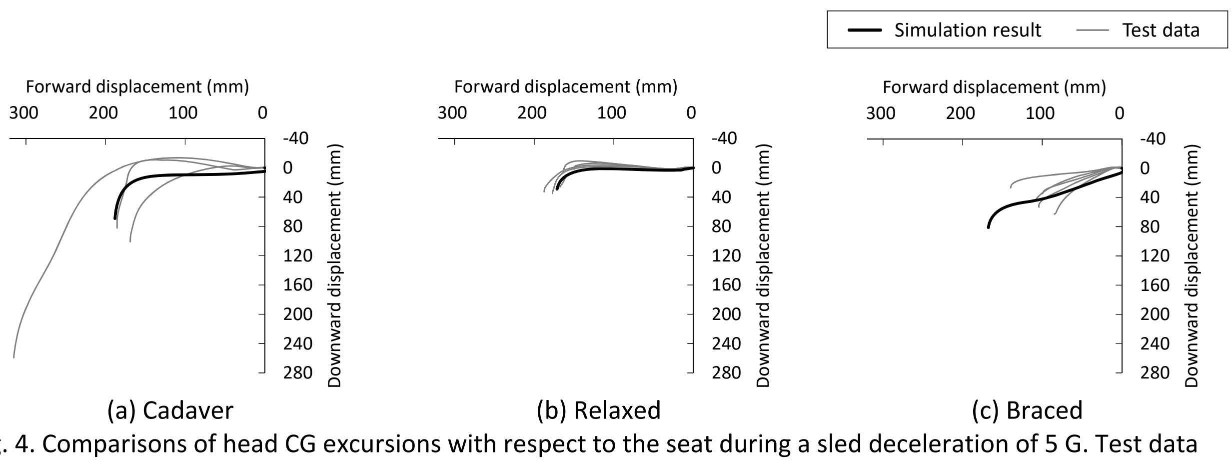

Fig. 4. Comparisons of head CG excursions with respect to the seat during a sled deceleration of 5 G. Test data are taken from [24].

Quantitative Evaluation using the CORA Method

The CORrelation and Analysis (CORA) method reported in [26-27] was applied for the quantitative evaluation of the validation results. The CORA method combines two independent sub-methods: corridor rating and cross-correlation rating. The corridor method evaluates the fitting of a response curve to automatically calculated corridors. The cross-correlation method evaluates the cross-correlation function, size, and phase shift. We used CORA release 3.6 and its default parameters, except for A_EVAL, which adjusts the evaluation interval for each test. In the cross-correlation method, the weights are 0.50, 0.25, and 0.25 for cross-correlation function, size, and phase shift, respectively. In the overall evaluation, the weights for the corridor method and cross-correlation method are both 0.50. The evaluation using the CORA method is performed by rating between 1 and 0. The following sliding scale is defined by the technical report ISO/TR 9790: CORA ratings of 0.86 to 1.0, 0.65 to 0.86, 0.44 to 0.65, 0.26 to 0.44, and 0.0 to 0.26 are evaluated as Excellent, Good, Fair, Marginal, and Unacceptable, respectively.

Table IV summarises the results of quantitative evaluation for validations performed in this study using the CORA method. Since only time-history curves are available in CORA 3.6, Table IV shows only the evaluation of validation results with the time-history curve. Although the quantitative evaluation results of thoracic deflections against thoracic-belt compression were Marginal or Unacceptable in points No. 4, 5, and 6, where the deflection magnitudes were small, other evaluation results were better than Fair.

TABLE IV

QUANTITATIVE EVALUATION RESULTS OBTAINED USING THE CORA METHOD

Test condition [Physical quantity]	Model	Point	Corridor method rating	Correlation method: Cross correlation	Correlation method: Size	Correlation method: Phase shift	Correlation method rating	Total rating	Evaluation
Thoracic belt compression [Deflection]	AF05	No.1	0.683	0.954	0.694	0.999	0.900	0.792	Good
		No.2	0.557	0.920	0.606	0.702	0.787	0.672	Good
		No.3	0.793	0.978	0.790	1.000	0.936	0.865	Excellent
		No.4	0.535	0.329	0.113	0.000	0.193	0.364	Marginal
		No.5	0.265	0.071	0.460	1.000	0.394	0.330	Marginal
		No.6	0.167	0.934	0.171	0.000	0.510	0.338	Marginal
		No.7	0.272	0.864	0.331	0.677	0.684	0.478	Fair
		No.8	0.739	0.832	0.787	0.915	0.841	0.790	Good
	AM50	No.1	0.744	0.955	0.746	1.000	0.910	0.827	Good
		No.2	0.860	0.964	0.863	0.900	0.928	0.894	Excellent
		No.3	0.455	0.954	0.492	1.000	0.850	0.653	Good
		No.4	0.170	7.270	0.206	1.000	0.301	0.236	Unacceptable
		No.5	0.116	0.072	0.094	1.000	0.310	0.213	Unacceptable
		No.6	0.172	0.877	0.251	0.000	0.501	0.337	Marginal
		No.7	0.410	0.893	0.466	0.700	0.742	0.576	Fair
		No.8	0.683	0.921	0.853	1.000	0.924	0.803	Good
	AM95	No.1	0.801	0.958	0.816	1.000	0.933	0.867	Excellent
		No.2	0.310	0.863	0.389	1.000	0.779	0.545	Fair
		No.3	0.499	0.953	0.622	1.000	0.882	0.691	Good
		No.4	0.235	1.780	0.742	1.000	0.436	0.335	Marginal
		No.5	0.141	0.091	0.177	1.000	0.340	0.240	Unacceptable
		No.6	0.197	0.935	0.204	0.000	0.519	0.358	Marginal
		No.7	0.422	0.878	0.526	1.000	0.821	0.621	Fair
		No.8	0.754	0.915	0.883	1.000	0.928	0.841	Good

Test condition [Physical quantity]	Model	Velocity / Deceleration	Corridor method rating	Correlation method: Cross correlation	Correlation method: Size	Correlation method: Phase shift	Correlation method rating	Total rating	Evaluation
Knee frontal impact [Force]	AF05	1.2 m/s	0.334	0.924	0.299	1.000	0.787	0.561	Fair
		3.5 m/s	0.399	0.457	0.635	1.000	0.637	0.518	Fair
		4.9 m/s	0.319	0.347	0.780	1.000	0.619	0.469	Fair
	AM50	1.2 m/s	0.488	0.845	0.496	1.000	0.797	0.642	Fair
		3.5 m/s	0.682	0.868	0.776	1.000	0.878	0.780	Good
		4.9 m/s	0.662	0.842	0.822	1.000	0.876	0.769	Good
	AM95	1.2 m/s	0.591	0.898	0.629	1.000	0.856	0.723	Good
		3.5 m/s	0.656	0.762	0.943	1.000	0.867	0.761	Good
		4.9 m/s	0.617	0.761	0.882	1.000	0.851	0.734	Good
frontal sled [Steering force]	AM50	2.5 G	0.623	0.811	0.934	1.000	0.889	0.756	Good
		5.0 G	0.559	0.766	0.657	0.824	0.753	0.656	Good
frontal sled [R pedal force]	AM50	2.5 G	0.462	0.715	0.595	1.000	0.756	0.609	Fair
		5.0 G	0.647	0.935	0.692	1.000	0.891	0.769	Good

Simulation Setups of a Frontal Collision after Brake Deceleration

In this paper, a frontal collision scenario in which AEBs were operated was simulated using THUMS Version 6 and a vehicular sled FE model. The vehicular sled FE model includes a Ford Taurus vehicle body, an automotive seat, a 3-point seatbelt, pedals, and a steering wheel with an airbag for drivers. The sled model was originally developed by the National Crash Analysis Center of the George Washington University under a contract with the Federal Highway Administration and National Highway Traffic Safety Administration of the United States Department of Transportation. The model was modified by the JSOL Corporation (Japan). The THUMS model was seated on the automotive seat with the seatbelt fastened, the hands were placed on the steering wheel, the feet were placed on the pedal and footrest, and gravity was added, as shown in Figure 5(a).

As shown in Figure 5(b), the THUMS model was exposed to a deceleration of 0.8 G by AEBs for 300 ms before the crash and then exposed to a deceleration due to frontal collision at a velocity of 55 km/h. As safety devices, the airbag was deployed 10 ms after the collision, and the seatbelt force limiter limited the belt tension to 4,000 N at the maximum. Furthermore, in this study, we investigated the effect of the seatbelt pre-pretension (PPT) that restrains the posture change of the driver during AEB operation before collision. The timing of PPT operation was determined with reference to [28], and the maximum tension of PPT was set to 200 N based on [29].

AF05, AM50, and AM95 were used as the THUMS model, and three muscle conditions – sleeping, relaxed, and braced – were applied to each model by using the muscle-activation controller. The PID gains for the controller data in Table III were used in the simulations. The purpose of the simulations is to investigate how body size, muscle activation, and PPT affect driver kinematics and injuries.

Analyses of Simulation Results

Driver Kinematics

Forward displacements of target markers at the head top, centre of gravity (CG) of the head, first cervical vertebra (C1), first thoracic vertebra (T1), and sacrum, as shown in Figure 6, were obtained from simulation results. In this study, the displacements of each marker with respect to the seat immediately before the airbag deployment, which occurred 310 ms after the AEB operation and 10 ms after the collision, were used for comparisons of driver kinematics.

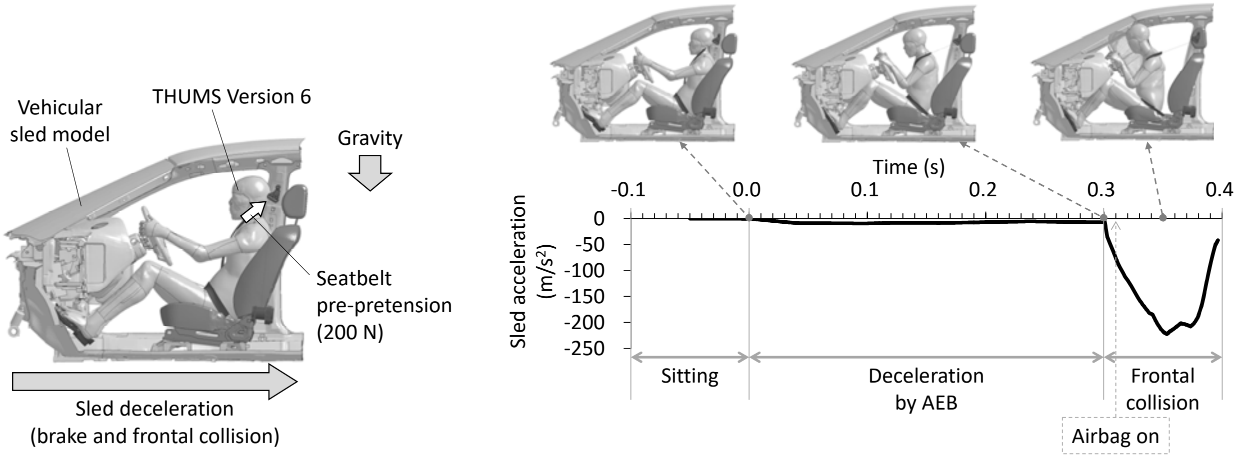

(a) Human and vehicular sled model (b) Sled deceleration

Fig. 5. Simulation setups for a frontal collision after deceleration by AEBs.

Chest Injury

It is commonly understood that mid-sternum deflection is correlated with rib fracture risk. As shown in Figure 7, in this study, the deflection was measured as the change of the anterior–posterior distance between the sternum and the thoracic vertebrae, which were under the path of the shoulder belt. At this time, considering the shear deformation of the ribs, the shortest distance between the sternum and the eighth thoracic vertebra (T8) to the eleventh thoracic vertebra (T11) was adopted as the anterior–posterior distance. To eliminate the influence of body size, the rate of deflection from the initial width was used for comparisons.

Internal Organ Injury

In this study, we evaluated injuries to the heart and liver, which were under the path of the shoulder belt, among internal organ injuries. As injury indicators, we used the critical volume fraction (CVF) with the threshold value of tensile strain set to 30%, which was used as a reference value for injury predictions using THUMS Version 4 [4].

Brain Injury

Reference [30] proposed the use of the cumulative strain damage measure (CSDM) calculated using a brain FE model as an indicator of brain injury. CSDM represents the cumulative volume fraction of brain tissue elements that exceed a pre-determined threshold of the maximum principal strain. It is commonly understood that the threshold of CSDM varies depending on the model. In this study, CSDM 25% (CSDM25), in which 25% is the threshold of the maximum principal strain, was used tentatively as an indicator of brain injury by referring to [30].

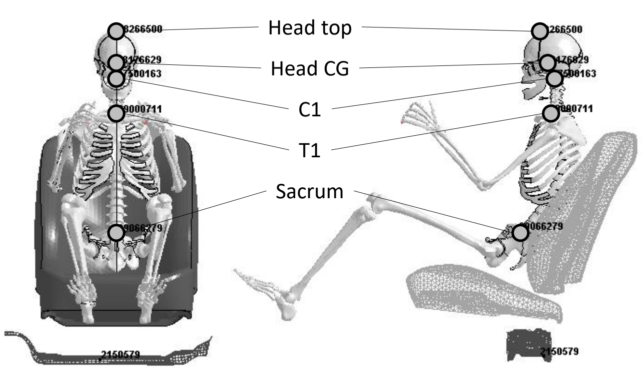

Fig. 6. Positions of target markers to measure forward displacements.

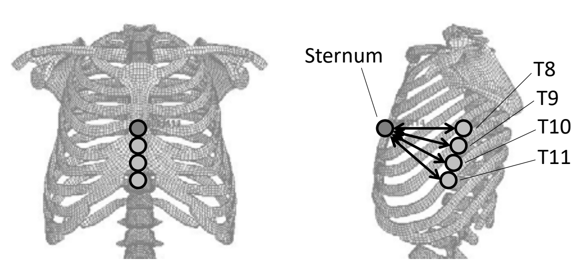

Fig. 7. Measurement positions of chest deflection.

III. RESULTS

The following sub-section presents simulation results indicating the effects of seatbelt PPT, muscle conditions, and body sizes on driver kinematics and injury outcomes.

Effect of Seatbelt Pre-pretension

To investigate the effect of seatbelt PPT, we compared simulation results for a relaxed AM50 driver between cases with and without PPT operation. Figure 8 shows comparisons of driver kinematics. The forward displacement of each target marker before airbag deployment was smaller with PPT operation. Comparisons of chest deflections and brain CSDM25 caused by the collision between the two cases are shown in Figures 9 and 10, respectively. The chest deflection in the case with PPT operation was more than that without PPT operation while the CSDM25 in the case with PPT operation was zero without any brain injury, less than that without PPT operation.

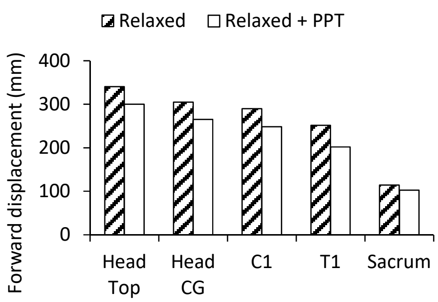

Fig. 8. Comparison of forward displacements with/without PPT (AM50, relaxed driver).

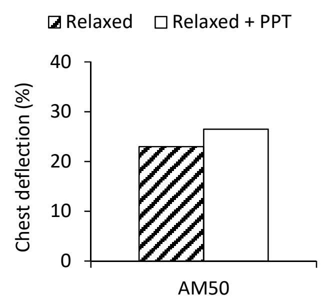

Fig. 9. Comparison of chest deflection with/without PPT (AM50, relaxed driver).

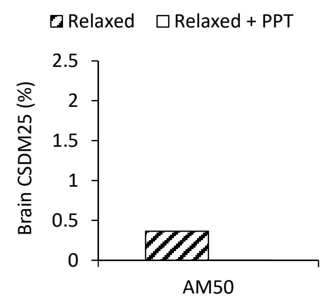

Fig. 10. Comparison of brain CSDM25 with/without PPT (AM50, relaxed driver).

Comparison of Seatbelt Pre-pretension for Braced Muscles

As mentioned above, PPT reduced the forward displacement of the driver's body. It is known from previous studies [1-2] that changes in the driver's posture are suppressed by muscle tension. Therefore, to investigate the difference between these constraint effects, simulation results of a relaxed driver with PPT were compared to those of a braced driver. There was no large difference in driver kinematics, as shown in Figure 11. At the same time, as shown in Figure 12, the chest deflection of the braced driver was less than that of the relaxed driver with PPT. On the other hand, as shown in Figure 13, the brain CSDM25 of the braced driver was more than that of the relaxed driver with PPT.

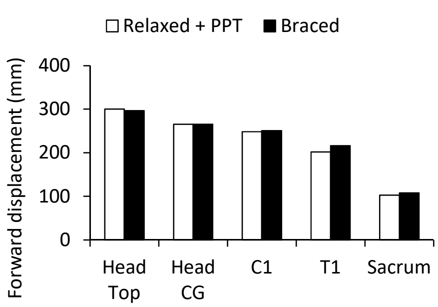

Fig. 11. Comparison of forward displacements between a relaxed driver with PPT and a braced driver (AM50).

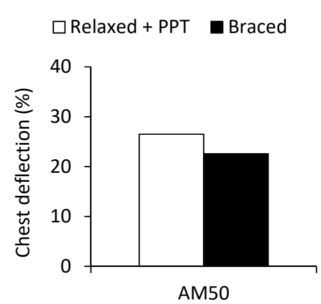

Fig. 12. Comparison of chest deflection between a relaxed driver with PPT and a braced driver (AM50).

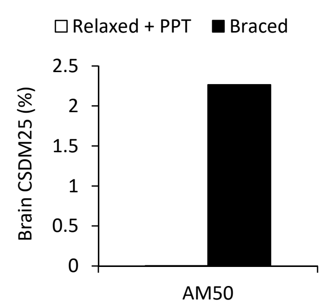

Fig. 13. Comparison of brain CSDM25 between a relaxed driver with PPT and a braced driver (AM50).

Effect of Muscle Activation under Conditions of Seatbelt Pre-pretension

PPT operates regardless of the driver's condition. We investigated the effect of muscle activity when PPT is in operation. As shown in Figure 14, the difference in forward displacement of the sacrum when PPT is in operation is small between a relaxed driver and a sleeping driver. However, the displacements of the sleeping driver became larger than those of the relaxed driver when approaching the head. In addition, the displacements of the braced driver are the smallest among the three drivers. Furthermore, the chest deflection of the sleeping driver was the greatest among the three drivers and that of the braced driver was the smallest, as shown in Figure 15. However, Figure 16 shows that there is not much difference in the maximum seatbelt contact forces among three drivers.

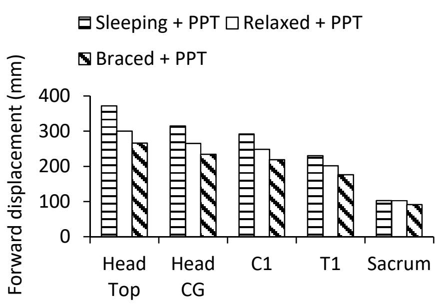

Fig. 14. Comparison of forward displacements between a sleeping and relaxed driver with PPT (AM50).

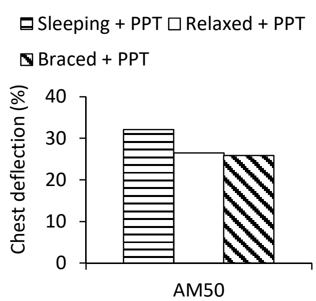

Fig. 15. Comparison of chest deflection between a sleeping and relaxed driver with PPT (AM50).

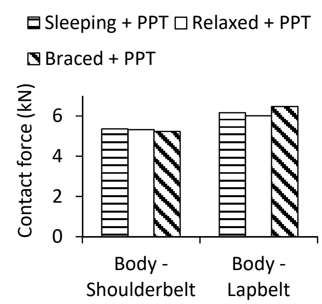

Fig. 16. Comparison of maximum seatbelt contact forces between a sleeping and relaxed driver with PPT (AM50).

Effect of Body Size

To investigate the effect of body size, Figure 17 shows comparisons of chest deflection among the models with the three body sizes under three conditions: sleeping and relaxed drivers with PPT and a braced driver. The chest deflections of AM95 were less than those of AM50 under all three conditions, and the chest deflection of AM95 under the braced condition was the lowest. The tendencies of the chest deflections for AM50 and AM95 are consistent with the trend of the heart and liver injury indicators shown in Figures 18 and 19, respectively. On the other hand, when including AF05, the chest deflection of AF05 was the greatest, as shown in Figure 17. Overall, the heart CVFs were higher than the liver CVFs.

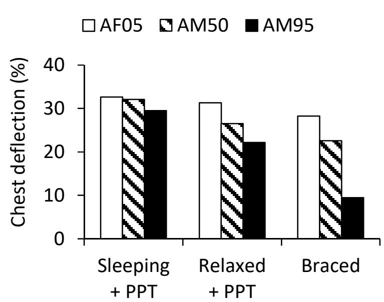

Fig. 17. Comparison of chest deflections among three body sizes.

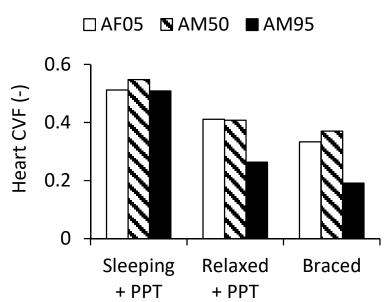

Fig. 18. Comparison of heart CVFs among three body sizes.

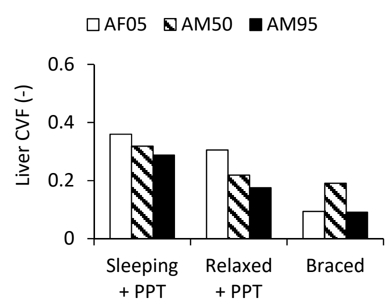

Fig. 19. Comparison of liver CVFs among three body sizes.

IV. DISCUSSION

Effect of Seatbelt Pre-pretension and Muscle Activation

Seatbelt PPT is intended to improve occupant protection performance in collisions by restraining the occupant more quickly compared to the case without seatbelt PPT. This study confirmed that the forward displacement of the relaxed driver was small when PPT was operated, as shown in Figure 8. By suppressing the occupant displacement, it is considered that the collision speed between the human body and the interior parts of the vehicle decreases and the injury risk caused by such secondary collisions is reduced. However, the chest deflection was great when PPT was operated, as shown in Figure 9. It is considered that the increase in the chest deflection is attributed in part to the increase in seatbelt contact forces due to PPT. On the other hand, Figure 10 suggests that the risk of brain injury is less when PPT is operated. It was found from Figure 11 that muscle tension has an effect of suppressing the forward displacement equivalent to PPT. The chest deflection of the braced driver in Figure 12 was less than that of the relaxed driver without PPT in Figure 9. The simulation results suggest that muscle tension is more effective for reducing the risk of chest injury than PPT. On the other hand, Figure 13 shows that muscle tension may increase the risk of brain injury.

PPT can function as an alarm warning the driver of the collision. When the driver detects the collision with the help of PPT, the resulting muscle tension might alleviate the chest injury. It is also considered that PPT can wake up sleeping drivers. Even under the conditions in which PPT functions, it can be confirmed from Figures 14 and 15 that muscle conditions could change driver kinematics and chest deflections. The simulation results suggest that the risk of chest injury can be reduced by waking up the driver before the collision. However, muscle tension also has the potential to increase the risk of brain injury as shown in Figure 13. Further studies are needed to investigate effects of muscle tension on brain injuries using THUMS Version 6 and more detailed brain models.

Effect of Body Size

AM95 showed lower injury risks to the chest, heart, and liver compared to AM50, as shown in Figures 17, 18, and 19. Since the skin and fat layers are thicker in AM95, it is reasonable to consider that the injury risks were reduced as a result of the impact energy being absorbed by them. In addition, we consider that the effect of PPT in AM95 was difficult to distinguish. Since AM95 is heavier, the contribution of energy reduction by the ride-down effect is relatively small. On the other hand, it is considered that the restraining effect on the skeleton caused by the seatbelt was reduced by the deformation of the soft tissue. The comparison among three conditions including AF05 in Figure 17 indicates that AF05 showed the greatest chest deflection. As mentioned previously, muscular forces were set to be smaller in AF05 than in AM50 and AM95. It seems that this effect was reflected in the results. Moreover, we calculated the heart and liver CVFs, as shown in Figures 18 and 19. Because these internal organs were under the seatbelt path, they showed tendencies generally similar to that of chest deflection.

Validation and Validity

In the validation analysis of kinematic response considering muscle activation, we adjusted controller parameters to reproduce the head excursions of volunteers. However, the head excursion of a braced driver represented using the muscle controller was greater than that of the volunteer data, as shown in Figure 4(c). This is probably because the steering column force before the input of acceleration of 5G was smaller than that in the tests as shown in Figure A14(a) of Appendix. Further improvement of the muscle-activation controller or an adaptation of controller parameters is necessary to show the quantitative validity of the result.

The scaling method is useful to consider effects of the body size and mass on impact responses. For the validation graph of the thoracic frontal impact shown in Figure A2 of Appendix, the scale factors of each body size for each physical value was calculated using the method in [31], and the simulation results were scaled. Table V and Figure 20 present the scale factors and scaling results. These scale factors were calculated using the average value of cadaver data used for creation of corridor. Figure 20 shows that the peak value of force in AF05 considering the scaling is greater than that predicted by AF05 of THUMS Version 6 in Figure A2. This is probably because material characteristics of the breast of women different from men were taken into consideration in AF05 of THUMS Version 6. This scaling method is useful to investigate differences in body sizes but it requires detailed experimental data, and to our knowledge, this method has not been applied to belt compression tests used for validations of THUMS Version 6.

TABLE V
SCALE FACTORS FOR THE SIMULATION RESULT OF VALIDATION OF THE THORACIC FRONTAL IMPACT

Body size	Scale factor	
	Deflection	Force
AF05	1.00	1.17
AM50	1.00	0.89
AM95	0.97	0.79

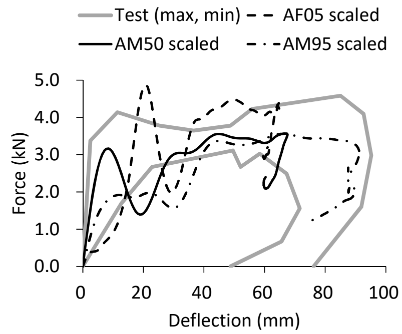

Fig. 20. Comparison of the thoracic force–deflection relationship between scaled simulation results and test data, which are taken from [15].

V. CONCLUSIONS

We developed a family of human FE body models called THUMS Version 6, which has three body sizes: AM50, AF05, and AM95. The models were validated against cadaveric impact or compression responses and AM50 model was validated against male volunteers' kinematic responses considering active portion. We applied muscle-activation controllers developed in our previous studies to predict occupant kinematics and injury outcomes of three muscle conditions: sleeping, relaxed, braced drivers. Simulation results for a frontal collision at 55 km/h after a deceleration of 0.8 G by AEBs for 300 ms showed that injury outcomes differed among the drivers with the three muscle-activation conditions for each body size. Simulation results also showed PPT operation decreased occupant forward displacements and brain injury risks but increased chest injury risks while muscle tension decreased occupant forward displacements and chest injury risks but increased brain injury risks. Although further studies are necessary to improve adaptation of muscle-activation controller parameters in the validation on the volunteers' head kinematics and investigate effects of muscle tension on brain injury risks, the models have the potential to predict occupant injury risks under different muscle-activation conditions in frontal collisions with pre-crash deceleration.

VI. ACKNOWLEDGEMENT

The authors thank Dr Tsuyoshi Yasuki, Dr Yuichi Kitagawa, Shigeki Hayashi, and Hiroshi Miyazaki of Toyota Motor Corporation (Japan) for their kind and enduring assistance in this research.

VII. REFERENCES

[1] Ejima S, Zama Y, Satou F, Holcombe S, Ono K, Kaneoka K, Shiina I. Prediction of the physical motion of the human body based on muscle activity during pre-impact braking. *Proceedings of IRCOBI Conference*, 2008, Bern, Switzerland.

[2] Beeman SM, Kemper AR, Madigan ML, Duma SM. Effects of bracing on human kinematics in low-speed frontal sled tests. *Annals of Biomedical Engineering*, 2011, 39(12):2998-3010.

[3] Untaroiu C, Lim JY, Shin J, Crandall J, Malone DP, Tannous RE. Evaluation of a finite element model of the THOR-NT dummy in frontal crash environment. *Proceedings of the 21st ESV Conference*, 2009, Stuttgart, Germany.

[4] Shigeta K, Kitagawa Y, Yasuki T. Development of next generation human body FE model capable of organ injury prediction. *Proceedings of the 21st ESV Conference*, 2009, Stuttgart, Germany.

[5] Gayzik FS, Moreno DP, Vavalle NA, Rhyne AC, Stitzel JD. Development of a full human body finite element model for blunt injury prediction utilizing a multi-modality medical imaging protocol. *Proceedings of the 12th International LS-DYNA Users Conference*, 2012, Dearborn, Michigan, USA.

[6] Kitagawa Y, Yasuki T. Correlation among seatbelt load, chest deflection, rib fracture and internal organ strain in frontal collisions with human body finite element models. *Proceedings of IRCOBI Conference*, 2013, Gothenburg, Sweden.

[7] Guleyupoglu B, Schap J, Kusano KD, Gayzik FS. The effect of precrash velocity reduction on occupant response using a human body finite element model. *Traffic Injury Prevention*, 2017, 18(5):508-514.

[8] Meijer R, Broos J, Elrofai H, de Bruijn E, Forbes P, Happee R. Modelling of bracing in a multi-body active human model. *Proceedings of IRCOBI Conference*, 2013, Gothenburg, Sweden.

[9] Östh J, Brolin K, Bråse D. A human body model with active muscles for simulation of pretensioned restraints in autonomous braking interventions. *Traffic Injury Prevention*, 2015, 16:304-313.

[10] Iwamoto M, Nakahira Y, Tamura A, Kimpara H, Watanabe I, Miki K. Development of advanced human models in THUMS. *Proceedings of the 6th European LS-DYNA Users' Conference*, 2007, Gothenburg, Sweden.

[11] Iwamoto M, Nakahira Y, Kimpara H. Development and validation of the Total HUman Model for Safety (THUMS) toward further understanding of occupant injury mechanisms in precrash and during crash. *Traffic Injury Prevention*, 2015, 16(sup1):S36-S48.

[12] Kato D, Nakahira Y, Iwamoto M. A study of muscle control with two feedback controls for posture and reaction force for more accurate prediction of occupant kinematics in low-speed frontal impacts. *Proceedings of the 25th ESV Conference*, 2017, Detroit, Michigan, USA.

[13] Winters JM, Woo SLY (eds.). Multiple Muscle Systems: Biomechanics and Movement Organization, pages 69-93 and 726-749, *Springer-Verlag*, New York, USA, 1990.

[14] Iwamoto M, Nakahira Y, Kimpara H, Min K. Development of a finite element model of 5th percentile female with multiple muscles and its application to investigation on impact responses of elderly females. *Proceedings of the 23rd ESV Conference*, 2013, Seoul, Republic of Korea.

[15] Kroell CK, Schneider DC, Nahum AM. Impact tolerance and response of the human thorax II. *Proceedings of the 18th Stapp Car Crash Conference*, SAE Technical Paper 741187, 1974, Ann Arbor, Michigan, USA.

[16] Shaw JM, Herriott RG, McFadden JD, Donnelly BR, Bolte JH. Oblique and lateral impact response of the PMHS thorax. *Stapp Car Crash Journal*, 2006, 50:147-167.

[17] Viano DC. Biomechanical responses and injuries in blunt lateral impact. *Proceedings of the 33rd Stapp Car Crash Conference*, SAE Technical Paper 892432, 1989, Washington, DC, USA.

[18] Cesari D, Bouquet R. Behaviour of human surrogates thorax under belt loading. *Proceedings of the 34th Stapp Car Crash Conference*, SAE Technical Paper 902310, 1990, Orlando, Florida, USA.

[19] Cavanaugh JM, Nyquist GW, Goldberg SJ, King AI. Lower abdominal tolerance and response. *Proceedings of the 30th Stapp Car Crash Conference*, SAE Technical Paper 861878, 1986, San Diego, California, USA.

[20] Foster CD, Hardy WN, Yang KH, King AI, Hashimoto S. High-speed seatbelt pretensioner loading of the abdomen. *Stapp Car Crash Journal*, 2006, 50:27-51.

[21] Bolte JH 4th, Hines MH, Herriott RG, McFadden JD, Donnelly BR. Shoulder impact response and injury due to lateral and oblique loading. *Stapp Car Crash Journal*, 2003, 47:35-53.

[22] Rupp JD, Miller CS, Reed MP, Madura NH, Klinich KD, Schneider LW. Characterization of knee-thigh-hip response in frontal impacts using biomechanical testing and computational simulations. *Stapp Car Crash Journal*, 2008, 52:421-474.

[23] Kryger MH, Roth T, Dement WC. Processing of somatic reflexes during sleep and wakefulness. *Principles and Practice of Sleep Medicine, sixth edition*, 2016, 243-244.

[24] Beeman SM, Kemper AR, Madigan ML, Franck CT, Loftus SC. Occupant kinematics in low-speed frontal sled tests: Human volunteers, Hybrid III ATD, and PMHS. *Accident Analysis and Prevention*, 2012, 47:128-139.

[25] Kato D, Nakahira Y, Iwamoto M. Development of a muscle controller for prediction of occupant kinematics in consideration of muscle tone conditions. *Transaction of JSAE (in Japanese)*, 2017, 48(6):1297-1302.

[26] Gehre C, Gades H, Wernicke P. Objective rating of signals using test and simulation responses. *Proceedings of the 21st ESV Conference*, 2009, Stuttgart, Germany.

[27] Gehre C, Stahlschmidt S. Assessment of dummy models by using objective rating methods. *Proceedings of the 22nd ESV Conference*, 2011, Washington, DC, USA.

[28] Mages M, Seyffert M, Class U. Analysis of the pre-crash benefit of reversible belt pre-pretensioning in different accident scenarios. *Proceedings of the 22nd ESV Conference*, 2011, Washington, DC, USA.

[29] Sander U, Mroz K, Bostrom O, Fredriksson R. The effect of pre-pretensioning in multiple impact crashes. *Proceedings of the 21st ESV Conference*, 2009, Stuttgart, Germany.

[30] Takhounts EG, Ridella SA, Hasija V, Tannous RE, Campbell JQ, Malone D, Danelson K, Stitzel J, Rowson S, Duma S. Investigation of traumatic brain injuries using the next generation of simulated injury monitor (SIMon) finite element head model. *Stapp Car Crash Journal*, 2008, 52:1-31.

[31] Mertz HJ. A procedure for normalizing impact response data. *SAE Technical Paper*, 1984, 840884.

VIII. APPENDIX

Validation of THUMS Version 6

Thoracic Frontal Impact

Cadaveric tests to investigate thoracic frontal impact responses were performed in [15(A1)]. In the tests, the impact was applied to the anterior surface of the thorax of a seated cadaver by using a cylindrical impactor with a diameter of 152 mm that simulated a steering-wheel hub. The displacement and acceleration of the impactor were measured to investigate the relationship between deflection and force. Figure A1 shows a simulation setup using AM50 to reproduce the test conditions. The mass and initial velocity of the impactor were 23 kg and 7.2 m/s, respectively. The vertical position at which the impact is applied was the sternum at the height of the fourth intercostal space, which is between the fourth and fifth ribs. According to the test conditions, the initial posture of the human-body model was seated, and its upper limbs were raised.

A comparison of the thoracic force–deflection relationship between simulation results and test data is shown in Figure A2. For a model of any body size, simulation results were generally within the range of the upper and lower limits of the test data. In addition, the maximum deflection of the thorax was the highest in AM95, followed by AM50 and AF05 in order.

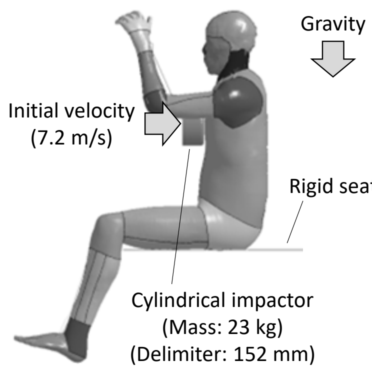

Fig. A1. Simulation setup using AM50 to reproduce the thoracic impact test.

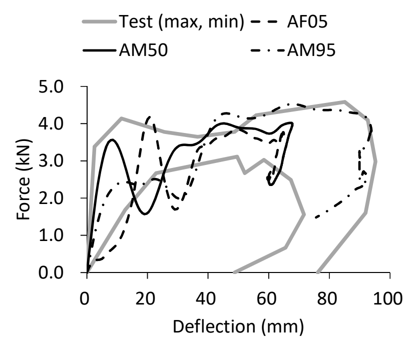

Fig. A2. Comparison of the thoracic force–deflection relationship between simulation results and test data, which are taken from [15].

Thoracic-Belt Compression

Cadaveric tests to investigate thoracic-belt compression responses were performed in [18]. In the tests, a pulling force was applied diagonally across the anterior surface of the thorax of a cadaver lying face upward on a test bench by using a shoulder belt. Thorax deflections at eight measurement points were measured while the belt was pulled. Figure A3 shows a simulation setup using AM50 of THUMS Version 6 to reproduce the test conditions. The back of the human model was pressed against the bench and brought into close contact with it. The pulling force was applied by an impactor with a mass of 22.4 kg, which was connected to the end of the belt. The belt-pulling velocity, estimated by differentiating the thorax displacement obtained from [18], was used as an input condition. Figure A4 shows the time history of the inputted belt-pulling velocity. Measurement points of thoracic deflection selected on the basis of the test conditions in [18] are shown in Figure A5.

Figure A6 shows comparisons between simulation results and test data on time-history curves of thoracic deflection at each measurement point. The black lines show simulation results corresponding to human models of each size, and the grey lines show cadaveric test data. In the test data, time-history data for only one test case were obtained from [18], and the maximum and minimum values of thoracic deflection among all test cases are shown in Figure A6. The calculation results are generally between the maximum and minimum values of the test data, except for measurement point No. 5.

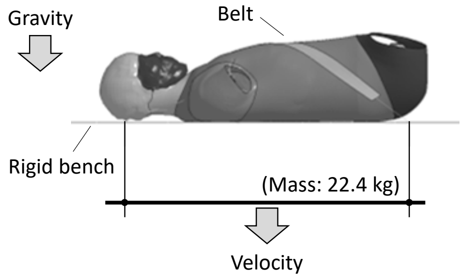

Fig. A3. Simulation setup using AM50 to reproduce the thoracic-belt compression test.

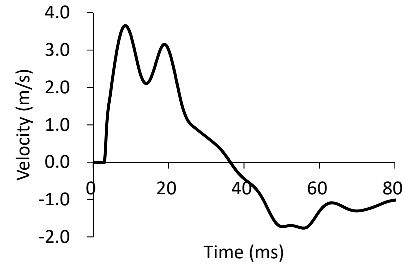

Fig. A4. Input data of belt-pulling velocity to reproduce the thoracic-belt compression test.

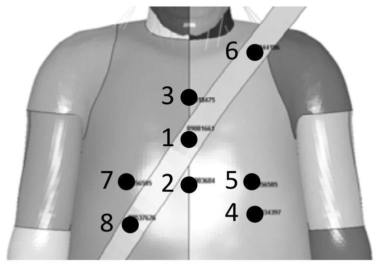

Fig. A5. Measurement points of thoracic deflection.

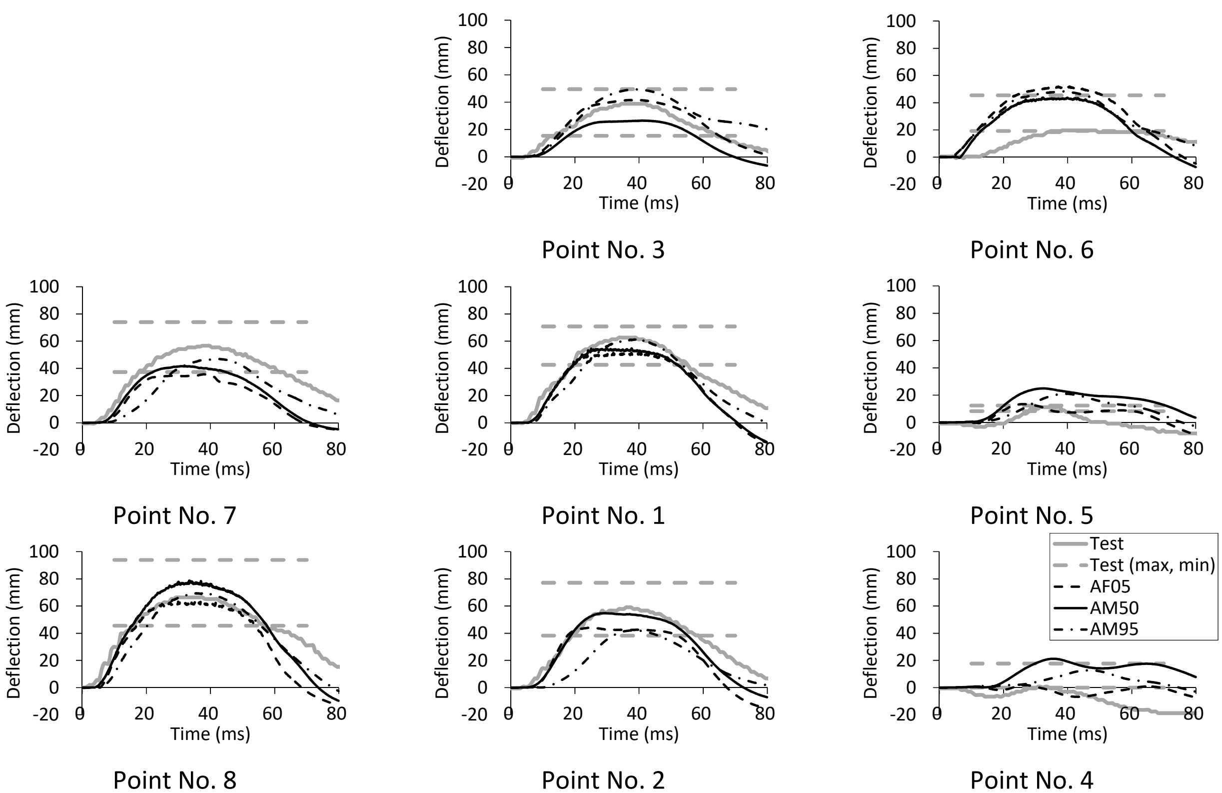

Fig. A6. Comparisons of thoracic deflection under belt compression. Test data are taken from [18].

Abdominal Frontal Impact

Cadaveric tests to investigate abdominal frontal impact responses were performed in [19]. In the tests, the impact was applied to the anterior surface of the abdomen of a seated cadaver by using a bar-shaped impactor with a diameter of 25 mm. In each test, the abdominal deflection with respect to the impactor force was recorded. Figure A7 shows a simulation setup using AM50 to reproduce the test conditions. The mass and initial velocity of the impactor were 32 kg and 6.1 m/s, respectively. The vertical position at which the impact is applied is at the height between the third lumbar vertebra and fourth lumbar vertebra. The impactor stroke was regarded as abdominal deflection.

A comparison of the abdominal force–deflection relationship between simulation results and test data is shown in Figure A8. The simulation result for AM95 was close to the upper limit of the test data. On the other hand, the impact forces of AF05 and AM50 were suddenly increased after the thoracic deflections reached almost 70 mm and 100 mm, respectively. The abdomens of AF05 and AM50 are thinner compared to that of AM95. The sudden increase in the force is considered due to the approach of the impactor to the spinal column.

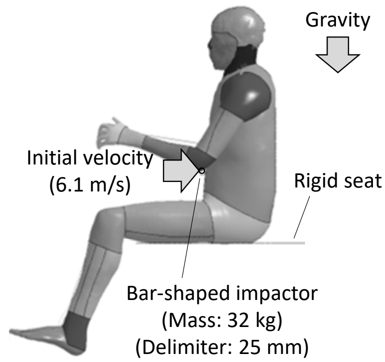

Fig. A7. Simulation setup using AM50 to reproduce the abdominal impact test.

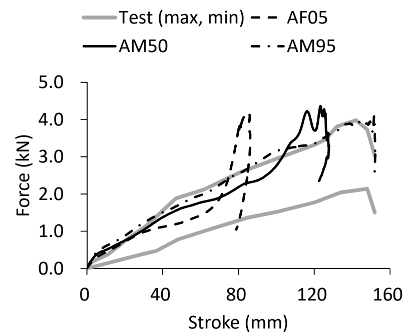

Fig. A8. Comparison of the abdominal force–deflection relationship between simulation results and test data, which are taken from [19].

Abdominal-Belt Compression

Cadaveric tests to investigate abdominal-belt compression responses were performed in [20]. In the tests, a pulling force was applied across the anterior surface of the abdomen of a cadaver by using a lap belt, and the pulling force and abdominal deflections were measured. Figure A9 shows a simulation setup using AM50 that reproduces the test conditions. Similar to thoracic compression, the back of the human model was brought into close contact with the bench before pulling the belt. The vertical position of the belt is at a height between the third and fourth lumbar vertebrae. Tests with three types of belt compression strengths using eight cadavers were conducted in [20]. AM50 and AM95 were validated by comparison with test-A, while AF05 was validated by comparison with test-C by using a cadaver with a size similar to the size of the model. Figure A10 shows time-history curves of the displacement given to the end of the belt in each test. Abdominal deflections are calculated as pulling strokes in this study.

Figure A11 shows comparisons between simulation results and test data of the relationship between forces and deflections at the abdomen. For AM50 and AM95, simulation results were generally within the upper and lower limits of the test data. On the other hand, for AF05, the force peak of the simulation result was approximately 4 kN and almost agreed with the test data.

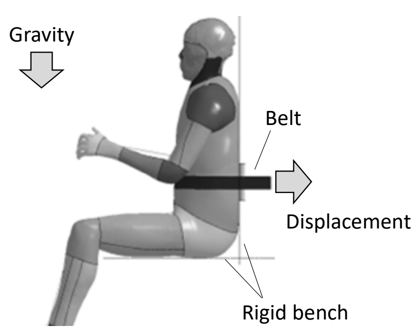

Fig. A9. Simulation setup using AM50 to reproduce the abdominal-belt compression test.

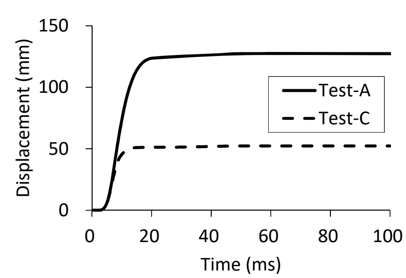

Fig. A10. Displacement–time curves of the belt to reproduce the abdominal-belt compression tests.

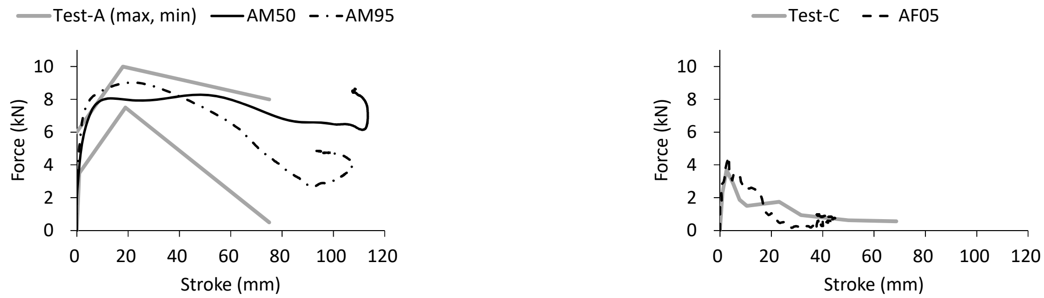

(a) Test-A, AM50 and AM95 (b) Test-C, AF05

Fig. A11. Comparisons of the relationship between force and deflection at the abdomen. Test data are taken from [20].

Knee Frontal Impact

Cadaveric tests to investigate knee frontal impact responses were performed in [22]. In the tests, the impact was applied to the knees of a cadaver by using an impactor with a mass of 255 kg. The initial velocity of the impactor was 4.9, 3.5, or 1.2 m/s, and the thickness of the pad attached to the impactor was 25 mm for initial velocities of 4.9 m/s and 3.5 m/s, and 38 mm for 1.2 m/s. The impactor force was measured using load cells located behind each impact surface. Figure A12 shows a simulation setup using the AM50 to reproduce the test conditions. The initial posture of the model was changed so that the angle of the knee joint was 90° according to the test condition.

Figure A13 shows a comparison of time-history curves of knee forces between simulation results and test data. For all the results corresponding to the three initial velocities, the magnitude of the maximum force was the highest in AM95, followed by AM50 and AF05 in order. AM95 showed results closest to the test data. The average body weight of the cadavers used in tests was 86.4 kg, which is approximately 10 kg heavier than the body weight of AM50. This is considered to be the reason why the results for AM95 were close to the test data.

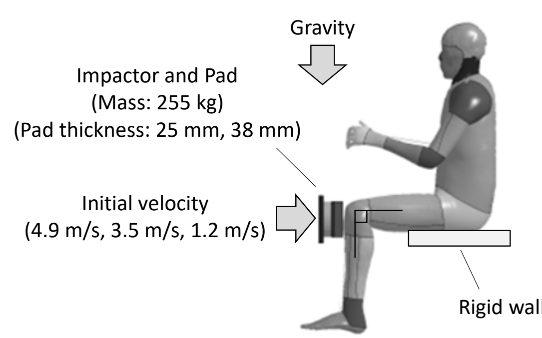

Fig. A12. Simulation setup using AM50 to reproduce the knee frontal impact test.

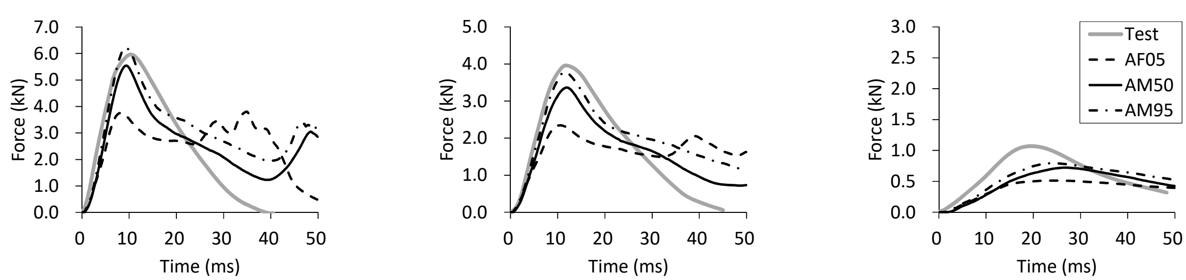

(a) 4.9 m/s (b) 3.5 m/s (c) 1.2 m/s

Fig. A13. Comparison of knee force under knee frontal impact. Test data are taken from [22].

Kinematic Response Considering Active Portion

Figure A14 shows the contact forces between the hands and steering wheel as well as between the right foot and footplate in the braced condition during a sled deceleration of 5 G. The time 0 s is defined as the time when the input of deceleration was started. In the simulations, the braced conditions were reproduced from 0.2 s before the input. Figure A14(a) shows the pushing forces on the steering wheel, and Figure A14(b) shows the pedalling force on the right footplate. These results were used for CORA evaluation.

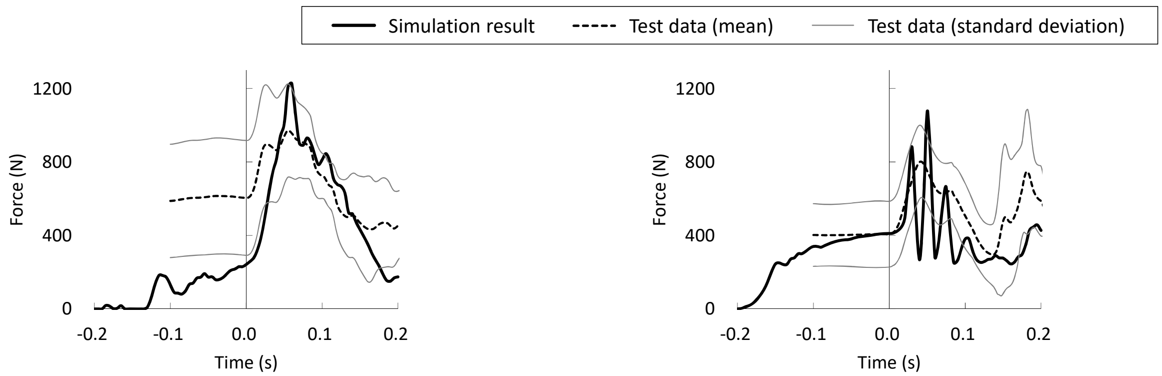

(a) Steering column force (b) Right footplate force

Fig. A14. Comparisons of contact forces of a braced driver during a sled deceleration of 5 G. Test data are taken from [23].

References in Appendix

[A1] Kroell CK, Schneider DC, Nahum AM. Impact tolerance and response of the human thorax. *Proceedings of the 15th Stapp Car Crash Conference*, SAE Technical Paper 710851, 1971, Coronado, California, USA.